Mater. Res. Soc. Symp. Proc. Vol. 845 © 2005 Materials Research Society AA9.7

Processing and Development of Nano-Scale HA coatings for Biomedical Application

Afsaneh Rabiei* and Brent Thomas**
Department of Mechanical and Aerospace Engineering,
**Department of Materials Science and Engineering,
North Carolina State University, Raleigh, NC, 27695-7910, U.S.A.

ABSTRACT

Functionally graded Hydroxyapatite coating with graded Crystallinity across the thickness of the film has been processed and tested as a more effective orthopedic/ dental implant coating. The present study aims to increase the service-life of an orthopedic/ dental implant by creating materials that form a strong, long lasting, bond with the Ti substrate as well as juxtaposed bone. The health relatedness of the new material is to increase bonding between an implant and juxtaposed bone so that a patient who has received joint or dental replacement surgery may quickly return to a normal active lifestyle. Cross-sectional transmission electron microscopy analysis displayed that the films have a graded crystal structure with the crystalline layer near the substrate and the amorphous layer at the top surface. Compositional analysis was performed using SEM-EDX at the top surface as well as STEM-EDX at the cross section of the film. The average calcium to phosphorous ratio at the surface is 1.46, obtained by SEM-EDX. The Ca/P ratios in the crystalline and amorphous layers of the film are 1.6 to 1.7, close to the ratio of 1.67 for HA.

INTRODUCTION

In order to improve the bioactivity of metal implants, Hydroxyapatite (HA: $Ca_{10}(PO_4)_6(OH)_2$) or is generally applied as a coating to the metal substrate [1]. This will cause a direct bonding and fast stabilization of implant because of HA's similarity with the inorganic components of human bone [2-4].

The bond strength of a coating layer with the metal substrate is an important factor to be considered seriously. Particulate debris at the bone prostheses interface with HA coated implants has been found to cause a foreign body response that is destructive to the surrounding tissues [5]. Dissolution rate of the implant must also be compatible with the rate of bone growth or otherwise the coating is not effective. The dissolution rate of crystalline HA has been observed to be very low, while that of the amorphous phase HA is considerably high [1].

Various techniques have been used to deposit calcium phosphate on metal substrates such as sputtering, electron beam deposition, laser deposition, and plasma spraying [6- 19]. So far, plasma spraying is the only technique being commercialized and most widely used because of its simplicity and cost effectiveness. Regardless of the processing technique, the amorphous HA generally has a high dissolution rate in aqueous solutions. Therefore, the HA coatings need to be subsequently heat-treated in order to convert the as deposited amorphous phase into a crystalline phase [16- 19 and 20]. However, the heat treatment increases the processing time and cost and can even cause residual stresses in the HA coating due to a thermal expansion mismatch between the coated layer and the metal substrate. This residual stresses may even lead to the cracking of the coating and eventual reduction in its bond strength [16- 19].

* Corresponding Author

In this study, in order to balance the benefits of crystalline and amorphous HA, films with graded crystallinity were prepared on silicon substrate using dual ion beam sputtering by manipulating deposition temperature. Several advantages over plasma spraying are expected in ion beam assisted deposition. First, the film bonds to substrate on an atomic level, which leads to better and more consistent adhesion strength than plasma sprayed coatings [21]. Secondly, the assist beam increases the degree of mixing between the film and substrate, further increasing adhesion strength [22]. The in-situ heat treatment allows the growth of films with various crystal structures without the need for post deposition annealing, which can impact the processing time and cost. Additionally, the HA coatings have been deposited as thin films from 1 to 2μm thick, much thinner than coatings applied using plasma spray technique. Thinner coatings can provide a higher interfacial strength and better fracture resistance than thicker plasma spray coatings.

Microstructure of graded HA films with less than 1 micron thickness were studied by various characterization techniques such as scanning electron microscope-energy dispersive spectroscope (SEM-EDX), transmission electron spectroscope (TEM) and field emission scanning electron microscope (STEM)-EDX.

EXPERIMENTAL PROCEDURES

HA films were prepared on silicon substrate in a dual ion beam sputtering system with a base pressure of 9×10^{-7} Torr. The primary ion source is an 8 cm Kaufman-type ion source used for sputtering and the secondary ion source is a 3 cm Kaufman-type ion source for ion bombardment.

Two HA ($Ca_{10}(PO_4)_6(OH)_2$, Cerac Inc., 99% purity) targets with different sizes and holders were used for the deposition. One was 12.7 cm diameter HA target bonded onto a copper holder (Target A) and the other was 15.24 cm diameter HA target recessed into a stainless steel holder (Target B). The depositions ran for 4.5 hours in all cases. For the duration of the runs, the primary source was at 1000 V and a gas flow of 3 sccm was provided to each ion source bringing the background pressure of the run to approximately 4×10^{-4} Torr. For the first 10 minutes of the runs, the assist beam was set at 1000 V to increase bombardment of the samples and improve film adhesion. After the first 10 minutes, the assist beam was set to 400 V, where it remained until the end of the runs. During the first 2 hours of the runs, the substrate heater was set at 700 °C to grow the crystalline portion of the film. After 2 hours, the substrate heater was set to 500 °C, and after 4 hours the heater was turned off. During the final 30 minutes of the runs the temperature fell to 250 °C. Detailed deposition conditions are summarized in Table 1. Microstructures of films prepared from Target A were observed by transmission electron microscope (TEM, Topcon 002B) and field emission scanning transmission electron microscope (FE-STEM, Hitachi HD 2000). The sample for TEM and STEM analysis was prepared using the in-situ lift-out technique associated with the FEI 200 Focused Ion Beam System.

Table 1. Summary of deposition condition

Step	Time	Assist Beam Voltage	Primary Beam Voltage	Substrate Temperature
1	0 - 10 min	1000 V	1000 V	700°C
2	10 - 120 min	400 V	1000 V	700°C
3	120 - 240 min	400 V	1000 V	500°C
4	240 - 270 min	400 V	1000 V	500 - 250°C

The surface film composition was evaluated using scanning electron microscope (S-3200N, Hitachi) equipped with an energy dispersive X-ray spectroscopy (EDX). The average surface composition was taken from six locations and is summarized in Table 2. Compositional analysis from the cross section of the film was performed by STEM-EDX (Hitachi HD 2000).

RESULTS AND DISCUSSION

HA is one of several calcium phosphate phases. There are other crystalline phases such as α- and β-tricalcium phosphate (TCP) and tetracalcium phosphate (TTCP). It is important to know the exact crystalline phases in the film since these phases have inferior osteocompatibility than HA coating due to their different crystal structures [23, 24]. X-ray diffraction pattern of the film on silicon substrate has been studied and presented elsewhere [25].

Cross sectional microstructure of the HA film on silicon substrate was examined by TEM and STEM and is shown in Figs. 1 and 2. The 875 nm thick HA film is including three main regions. The silicon wafer is covered by a thin amorphous layer of silicon dioxide about 12 nm thick, followed by a coarse crystalline HA layer 210 nm thick (Fig. 2 (b)). On the top of that, there is a fine crystalline layer 140 nm thick, followed by an amorphous layer at the top surface approximately 513 nm thick. The grain size and crystallinity gradually decrease toward the surface of the film as seen in Figs. 1 and 2. The microstructure reveals a very fine nano-scale columnar grain structure in the crystalline layers (Fig. 2). The selected area diffraction (SAD) patterns from various layers are presented elsewhere [25]. It is confirmed by SAD pattern study that the crystalline layers are corresponding to polycrystalline HA with (113), (213), (501) and (423) planes, while the top layer is an amorphous phase. The crystallinity of the film decreases towards the surface of the film. With the deposition rate (193 nm/hr) calculated from deposition time and film thickness, the amorphous layer is corresponding to steps 3 and 4 in Table 1, in which the deposition temperature was from 500°C to 250°C. Knowing that it is likely to form crystalline HA coatings above 500°C [13], the above mentioned substrate temperatures have been selected. Average surface compositional analysis has been conducted on all samples using SEM-EDX and the average value of six locations are presented in Table 2. Calcium, phosphorous and oxygen elements were identified in the film as well as argon. The Ar element found in the film is due to an entrapment of argon gas during ion beam bombardment. Approximately 3~5 at.% of copper was found in the sample deposited using the Target A. The introduction of copper was due to sputtering from the copper target holder resulting from divergence of the primary ion beam. Several efforts were made to eliminate introduction of copper into the film such as increasing the target diameter, and changing the target holder to stainless steel.

Table 2. Average top surface compositional analysis of the HA coating by SEM- EDX

Elements	Target A (at. %)	Target B (at. %)
Ca	13.54	12.99
P	9.29	9.21
O	71.96	76.30
Ar	2.05	1.15
Cu	3.18	-
Fe	-	0.36
Ca/P	1.46	1.41

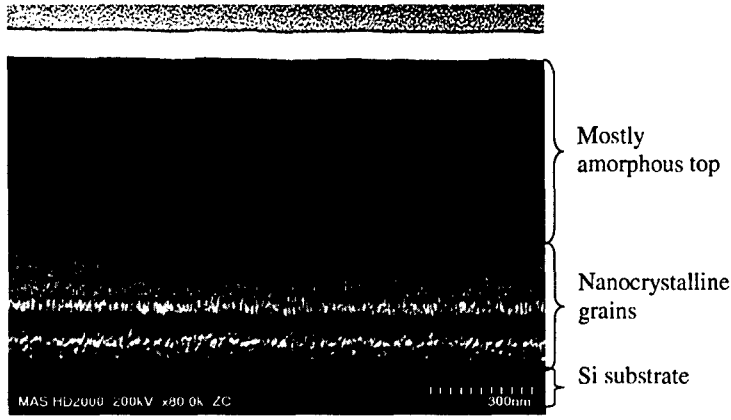

Fig. 1. STEM cross sectional image of HA film with graded crystal structure (The boxes in the figure are shown in Fig. 2).

This caused a complete elimination of copper content in the next set of depositions, but there was trace amount of some elements such as iron (less than 0.5 %) in the deposited films from Target B as can be seen in that Table 2. The average Ca/P ratios taken from the surface by SEM-EDX were 1.46 and 1.41 for the films sputtered from Target A and Target B, respectively. The Ca/P ratios of the films prepared by sputtering reported so far are in the wide ranges of 1.2-8.0 which differ from the value of 1.66 for pure HA [14-16]. For better understanding of elemental distribution of the graded structure, STEM-EDX analysis was done on the cross section of the film. Figure 1 is the z-contrast STEM image which shows the STEM-EDX locations. The Ca/P ratio varies with a distance from the interface between HA coating and silicon substrate. The Ca/P ratios from locations 1, 4 and 5 are all about 1.66 (similar to crystalline HA), while those from locations 2 and 3 are 1.0 and 1.5, respectively. It should be noted that the locations 1~4 are crystalline phases and location 5 is amorphous phase. Although, the Ca/P ratio for locations 2 and 3 are below that of HA (1.66), the SAD pattern confirmed the presence of HA in those layers. The Ca/P ratio is affected by several factors such as sputtering yields and sticking coefficients of elements. Different sputtering yields between elements may result in composition change of target with deposition time. P is known to be sputtered preferentially and more volatile than Ca, which means the phosphorous atoms are preferentially sputtered from the target and also resputtered from the film before they are settling in the film. In addition, it is reported that the Ca/P varies with substrate types (conducting or insulating) and deposition time, resulted from changing in substrate charging [15]. In this case, sharp decrease in the Ca/P ratio from location 1 to location 2 can be related to decreasing the secondary beam voltage from 1000 V to 400 V few minutes after beginning the deposition. As the secondary voltage decreases, resputtering rate of P in the film decreases, resulting in higher P and lower Ca/P ratio. This deficiency in Ca/P ratio is being recovered gradually during the run and specially by decreasing the substrate temperature. Increasing the film thickness during the run can contribute to less conductivity further temperature drop of substrate. Higher temperature of substrate contributes to more atomic mobility and may cause more resputtering of P from the film. Further study on compositional change with deposition time is being conducted.

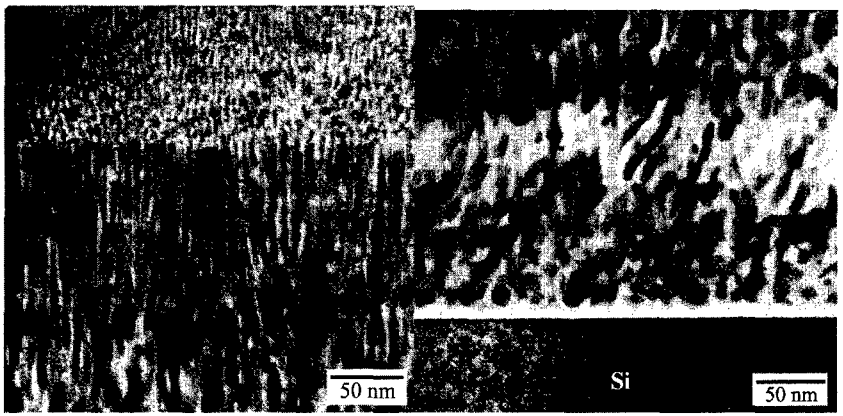

(a) (b)

Fig. 2. (a) Interfacial region between HA coating and silicon substrate and (b) high magnification TEM image showing nano columnar grains underneath amorphous region.

The graded crystal structure is expected to be ideal for implant osseointegration. The amorphous region of these films, at the top surface, should allow for rapid integration and cell growth, while the crystalline region, at the interface between the substrate and film, would be stable enough to resist dissolution until bone growth has reached the coating surface. The gradual decrease of the grain size and crystallinity towards the surface causes an increase in initial absorption of calcium from cerium leading to select protein adsorption to enhance bone cell function.

CONCLUSIONS

Functionally hydroxyapatite films deposited by dual ion beam sputtering were deposited with in-situ heat treatment by changing substrate temperatures during deposition. The substrate temperature decreased from 700°C to 250°C to manipulate the amount of crystalline phase in the film. The graded structure of the film was confirmed by cross sectional TEM and STEM studies. The region near substrate with a deposition temperature of 700°C, was composed of columnar nano-crystalline HA phase. The region at the top with a deposition temperature below 500°C was composed of an amorphous phase. The graded crystal structure is expected to be ideal for implant osseointegration. The amorphous region of these films, at the top surface will allow for rapid integration and cell growth, while the crystalline region, at the interface between the substrate and film would be stable enough to provide implant fixation. Compositional analysis was performed on the surface and the cross-section of the film by SEM-EDX and STEM-EDX, respectively. The average Ca/P ratio from the surface of the film was 1.46. Cross sectional analysis by STEM-EDX showed that the Ca/P ratio varied with film thickness. The Ca/P ratio decreased from 1.66 (the ratio of HA) to 1.0 when the secondary voltage decreased from 1000 V to 400 V. It might be attributed to decrease in the resputtering of P in the film. The Ca/P ratio is recovered to 1.66 in the crystalline and amorphous layers during further deposition period. Further study on the compositional analysis and percentage of crystallinity on various layers of the film is being conducted.

ACKNOWLEDGEMENTS

A part of this study is funded by a grant from the National Science Foundation (Grant No: 0402339). The authors would like to acknowledge very helpful discussions and the access to Dr. Jerry Cuomo's lab as well as Dr. Joo ong's very helpful discussions.

REFERENCES

1. W.R. Lacefield, Hydroxyapatite coating. Ann NY Acad Sci 523 (1988), pp. 72–80.
2. L.L. Hench, Bioceramics. J Am Ceram Soc 81 (1998), pp. 1705–1728.
3. W. Suchanek and M. Yoshimura, Processing and properties of hydroxyapatite-bases biomaterials for use as hard tissue replacement implants. J Mater Res 13 (1998), pp. 94–117.
4. R.Z. LeGeros, Biodegradation and bioresorption of calcium phosphate ceramics. Clin Mater 14 (1993), pp. 65–88.
5. S. Wang, W.R. Lacefield and J.E. Lemons, Interfacial shear strength and histology of plasma sprayed and sintered hydroxyapatite implants in vivo. Biomaterials 17 (1996), pp. 1965–1970.
6. K. van Dijk, H.G. Schaeken, J.G.C. Wolke and J.A. Jansen, Influence of annealing temperature on r.f. magnetron sputtered calcium phosphate coatings. Biomaterials 17 (1996), pp. 405–410.
7. J.L. Ong, L.C. Lucas, W.R. Lacefield and E.D. Rigney, Structure, solubility and bond strength of thin calcium phosphate coatings produced by ion beam sputter deposition. Biomaterials 13 (1992), pp. 249–254.
8. T.S. Chen and W.R. Lacefield, Crystallization of ion beam deposited calcium phosphate. J Mater Res 9 (1994), pp. 1284–1290.
9. M. Yoshinari, Y. Ohtsuka and T. Derand, Thin hydroxyapatite coating produced by the ion beam dynamic mixing method. Biomaterials 15 (1994), pp. 529–535.
10. J.M. Choi, Y.M. Kong, S. Kin, H.E. Kim, C.S. Hwang and L.S. Lee, Formation and characterization of hydroxyapatite coating layer on Ti-based metal implant by electron beam deposition. J Mater Res Soc 14 (1999), pp. 2980–2985.
11. R.K. Singh, F. Qian, V. Nagabushnam, R. Damodaran and B.M. Moudgil, Excimer laser deposition of hydroxyapatite thin films. Biomaterials 15 (1994), pp. 522–528.
12. C.M. Cotell, D.B. Chrisey, K.S. Grabowski and J.A. Spregue, Pulsed laser deposition of hydroxyapatite thin films on Ti–6Al–4V. J Appl Biomater 8 (1992), pp. 87–93.
13. P. Ducheyne, W.V. Raemdonck, J.C. Heughebaert and M. Heughebaert, Sturctural analysis of hydroxyapatite coating on titanium. Biomaterials 7 (1986), pp. 97–103.
14. Y.C. Tsui, C. Doyle and T.W. Clyne, Plasma sprayed hydroxyapatite coating on titanium substrates. Part 1: mechanical properties and residual stress levels. Biomaterials 17 (1998), pp. 2015–2029.
15. Z. Zyman, J. Weng, X. Liu, X. Zhang and Z. Ma, Amorphous phase and morphological structure of hydroxyapatite plasma coatings. Biomaterials 14 (1993),
16. H. Ji and P.M. Marquis, Effect of heat treatment on the microstructure of plasma-sprayed hydroxyapatite coating. Biomaterials 14 (1933), pp. 64–68.
17. J. Chen, J.G.C. Wolke and K. de Groot, Microstructure and crystallinity in hydroxyapatite coatings. Biomaterials 15 (1994), pp. 396–399.
18. F. Brossa, A. Cigada, R. Chiesa, L. Paracchini and C. Consonni, Post-deposition treatment effects on hydroxyapatite vacuum plasma spray coatings. J Mater Sci Mater Med 5 (1994), pp. 855–857.
19. J. Chen, W. Tong, Y. Coa, J. Feng and X. Zhang, Effect of atmosphere on phase transformation in plasma sprayed hydroxyapatite coatings during heat treatment. J Biomed Mater Res 34 (1997), pp. 15–20.
20. K.A. Gross, V. Gross and C.C. Berndt, Thermal analysis of amorphous phases in hydroxyapatite coatings. J Am Ceram Soc 81 (1998), pp. 106–112.
21. S. Ding, C. Ju, J. Lin, J. Biomedical Mater. Res. 44 (1999) 266.
22. H. R. Kaufman and R. S. Robinson, Operation of Broad-Beam Sources. Commonwealth Scientific Corporation Alexandria VA 1987 p. 116.
23. G. Lewis, Biomed. Mater. Eng. 10 (2000) 157.
24. Y. Cao, J. Weng, J. Chen, J. Feng, Z. Yang and X. Zhang, Biomaterials 17 (1996) 419.
25. A. Rabiei, B. Thomas, B. Neville, J. W. Lee, and J. Cuomo, Mat. Sci. & Eng. C, in review
26. Z. S. Luo, F. Z. Cui and W. Z. Li, J. Biomed. Mater. Res. 46 (1996) 80.
27. K. Ozeki, T. Yuhta, Y. Fukui and H. Aoki, Surf. Coat. Technol. 160 (2002) 54.

28. B. Feddes, A. M. Vredenberg, J. G. C. Wolke and J. A. Jansen, Surf. Coat. Technol. 185 (2004) 346.
29. K. van Dijk, H G. Schaeken, J. G. C. Wolke and J. A Jansen, Biomaterials 17 (1996) 405.